Crystallization of β-MnO_2 Nanowires in the Pores of SBA-15 Silicas: In Situ Investigation Using Synchrotron Radiation

Marianne Imperor-Clerc,[†] Dominique Bazin,[†,‡] Marie-Dominique Appay,[§] Patricia Beaunier,[§] and Anne Davidson*[,§]

Laboratoire de Physique des Solides (UMR 8502-CNRS), Bat. 510, Université Paris Sud, 91405 Orsay Cédex, France, LURE, Bat. 209D, Centre Universitaire Paris-Sud, 91405 Orsay, France, and Laboratoire de Réactivité de Surface (UMR 7609-CNRS), Université Pierre et Marie Curie, 4 place Jussieu, Tour 54-55, 75252 Paris Cédex 05, France

Received December 19, 2003. Revised Manuscript Received February 19, 2004

An original preparation method, called "two solvents" method, allows the production of MnO_2 nanowires patterned by SBA-15 silicas under mild conditions, with a preserved two-dimensional hexagonal structure, a 97% filling of the porosity by oxide nanowires, and a controlled microstructure. A comparison is made with Mn-loaded SBA-15 prepared by more conventional adsorption methods. In the latter case, MnO_x particles inside and outside the silica grains, empty and filled mesopores, and several Mn oxides (MnO_2, Mn_2O_3, and Mn_3O_4) were identified. Once the preparation method of Mn-loaded SBA-15 optimized, various X-ray scattering and adsorption techniques using synchrotron radiation were used to observe salient features of the MnO_2 nanowires crystallization in situ upon calcination. X-ray absorption at the Mn K edge shows that the oxidation state of manganese increases from (II) to (IV) between 80 and 120 °C. The oxidation of the Mn(II) salt occurs at a temperature lower than that necessary for bulk manganese nitrate (200 °C), which confirms its confinement within the SBA-15 pores. β-MnO_2 nanowires of defective pyrolusite type are identified by wide-angle diffraction. The comparison between diffraction results and simulations demonstrates that the nanowire diameter is similar to the mesopore diameter of the silica host. A small contraction of unit-cell parameters occurs upon the crystallization of β-MnO_2 nanowires. A parallel overall intensity increase observed in small-angle X-ray diffraction is the fingerprint of a homogeneously filled porosity.

Using the pores of SBA-15 silicas[1] as solid nanoreactors (or a mould) in which inorganic objects (clusters, nanospheres, and nanowires) can be grown is a topic of intense research. Various metals,[2−4] carbon,[5] and silicon[6] nano-objects have been obtained. Several oxides (of indium,[7] zirconium,[8] tungsten,[9] chromium,[10,11] cerium, nickel,[11] cobalt, copper, and iron[11,12]) and mixtures of manganese oxides (MnO_2, Mn_2O_3, and Mn_3O_4[11]) have also been patterned. Among the synthetic pathways that have been reported so far, some were not accessible in our laboratory (supercritical fluid inclusion for instance,[12] inclusion of materials within polymers and inorganic matrixes is well-established and has been proven by a number of research groups). Others imply either modifications of the silica host (by silylation or grafting of amino-silanes) or the specific use of microwave-digested mesoporous silicas, selected because more silanol groups are preserved on the silica surface than when the template is removed by calcination.[11] Furthermore, the mesopores are generally partially occupied by the inorganic objects. For instance, in ref 11, despite the specific use of microwave-digested SBA-15, only 40% of the mesoporous volume of the SBA-15 host was finally occupied by oxide particles. Obviously, the quality of subsequent studies performed on materials deriving from SBA-15 silicas would be greatly improved if one could define specific conditions leading to more homogeneous samples. This would also help under-

* To whom correspondence should be addressed. E-mail: davidson@ccr.jussieu.fr.

[†] Laboratoire de Physique des Solides (UMR 8502-CNRS), Université Paris Sud.

[‡] LURE, Centre Universitaire Paris-Sud.

[§] Laboratoire de Réactivité de Surface (UMR 7609-CNRS), Université Pierre et Marie Curie.

(1) Zhao, D.; Feng, J.; Huo, Q.; Melosh, N.; Fredrickson, G.; Chmelka, B.; Stucky, G. D. *Science* **1998**, *279*, 548.

(2) Liu, Z.; Sakamoto, Y.; Ohsuna, T.; Hiraga, K.; Terasaki, O.; Ko, C. H.; Shin, H. J.; Ryoo, R. *Angew. Chem., Int. Ed.* **2000**, *39*, 3107. (b) Zhang, Z.; Dai, S.; Blom, D. A.; Shen, J. *Chem. Mater.* **2002**, *14*, 965.

(3) Gross, A. F.; Diehl, M. R.; Beverly, C.; Richman, E. K.; Tolbert, S. H. *J. Phys. Chem. B* **2003**, *107*, 5475.

(4) Han, Y. J.; Kim, J. M.; Stucky, G. D. *Chem. Mater.* **2000**, *12*, 2068.

(5) Huang, L.; Wind, S. J.; O'Brien, S. P. *Nano Lett.* **2003**, *3*, 299.

(6) Coleman, N. R. B.; Morris, M. A.; Spalding, T. R.; Holmes, J. D. *J. Am. Chem. Soc.* **2001**, *123*, 187.

(7) Yang, H.; Shi, Q.; Tian, B.; Lu, Q.; Gao, F.; Xie, S.; Fan, J.; Yu, C.; Tu, B.; Zhao, D. *J. Am. Chem. Soc.* **2003**, *125*, 4724.

(8) Janssen, A. H.; Yang, C. M.; wang, Y.; Schüth, F.; Koster, A. J.; de Jong, K. P. *J. Phys. Chem. B* **2003**, *107*, 10552.

(9) Zhu, K.; He, H.; Xie, S.; Zhuang, X.; Zhou, W.; Jin, S.; Yue, B. *Chem. Phys. Lett.* **2003**, *377*, 317.

(10) Zhu, K.; Yue, B.; Zhou, W.; He, H. *Chem. Commun.* **2003**, 98.

(11) Tian, B.; Liu, X.; Yang, H.; Xie, S.; Yu, C.; Tu, B.; Zhao, D. *Adv. Chem.* **2003**, *15*, 1370.

(12) Crowley, T. A.; Ziegler, K. J.; Lyons, D. M.; Erts, D.; Olin, H.; Morris, M. A.; Holmes, J. D. *Chem. Mater.* **2003**, *15*, 3518.

10.1021/cm035353m CCC: $27.50
Published on Web 04/03/2004

standing how the structural features of the silica hosts relate to the nature and crystallinity of the inorganic objects patterned in their mesopores.

The goal of the present study was to obtain manganese oxides nanowires, homogeneous in nature, dimensions, and dispersion within the porous volume of SBA-15. Manganese oxides were chosen because some of them, labeled MnO_x hereafter, including MnO_2, Mn_2O_3, and Mn_3O_4, can be used as oxidation heterogeneous catalysts. For instance, Mn_2O_3 was recently used for the degradation of halogenated volatile organic compounds (VOC).[13] Furthermore, it has been reported that decreasing the size of MnO_x particles could improve their reactivity, particularly toward oxygen.[14] Finally, the use of SBA-15 silica moulds is not a drawback for catalytic applications because silica can be easily removed in basic solutions. The nanocasting of manganese oxides nanowires in SBA-15 silicas has already been described but only mixtures of different oxides were produced.[11] Another interest of manganese oxides is that all of them can be obtained by calcination in air starting from a Mn(II) precursor salt. Among Mn(II) salts, we have selected manganese chloride and nitrate because of their high solubility in water,[15] which was expected to help their introduction into the SBA-15 porosity. Furthermore, the thermal transformations experienced by these salts upon calcination, both unsupported and supported on silica, are well-documented.[16] For instance, upon increasing temperature, bulk $Mn(NO_3)_2{\cdot}4H_2O$ first transforms into MnO_2 near 200 °C, then into Mn_2O_3 between 600 and 950 °C, and finally into Mn_3O_4 above 950 °C. The main difficulties associated with the study of these phase transformations arise from the different polymorphs of each MnO_x oxide; for instance, up to 14 different polymorphs of MnO_2 are known.[17]

To optimize and understand better the nanocasting process in itself, two distinct series of samples were prepared and characterized. The first one was obtained using a conventional adsorption technique on three different silicas: a nonporous reference (Degussa, Aerosil 380) and two mesoporous SBA-15 obtained respectively without (SBA-A) and with hydrothermal treatment (100 °C, 3 days, SBA-B). The second series of samples was prepared with the same SBA-A and SBA-B silicas but using an original "two solvents" impregnation method. This method, based on a volume of aqueous solution set equal to the porous volume of the silica mould (determined by N_2 sorption), derives from incipient wetness impregnation techniques. A similar approach has been successfully used by M. Ledoux et al.[18] to homogeneously disperse Co and Fe salts into the porosity of carbon nanotubes and generate patterned $CoFe_2O_4$ nanoparticles by calcination. In the specific case of SBA-15 silica hosts, we have found it necessary to suspend dehydrated silicas in *n*-hexane, an organic solvent poorly miscible with water, before contacting them with an aqueous manganese nitrate solution of volume set equal to the silica porous volume. The two series of samples were investigated by combining textural (N_2 sorption), local (transmission electron microscopy, TEM, coupled with high resolution, HR, and energy-dispersive X-ray spectroscopy, EDXS), and structural information (X-ray diffraction at small, SAXS, and wide angles, WAXS). The samples obtained by adsorption are highly heterogeneous and contain the following: (i) MnO_x particles inside (nanowires) and outside the silica grains, (ii) both filled and empty mesopores, and (iii) different MnO_x oxides. In contrast, the samples obtained by the "two solvents" impregnation technique are quite homogeneous and contain β-MnO_2 nanowires confined within the porosity of the SBA-15 hosts.

Table 1. Chemical Analysis and N_2 Sorption Analysis of Selected Samples Calcined ex Situ at 400 °C

silica	Mn/Si[a] (at.)	S_{BET}[b] ($m^2{\cdot}g^{-1}$)	V_P[c] ($cm^3{\cdot}g^{-1}$)	D_{BJH}[d] (Å)
nonporous silica	0.1	380		
SBA-A		600	0.70	40
Mn-SBA-A ads.	0.2	497	0.60	39
Mn-SBA-A two solvents	0.5	19	0.02	
SBA-B		700	1.10	60
Mn-SBA-B ads.	0.4	587	1.00	58
Mn-SBA-B two solvents	0.5	402	0.60	60

[a] Chemical analysis performed at Solaize, CNRS, France. [b] Determined for $P/P^0 \approx 0.08-0.25$, expressed by g of catalyst. [c] Measured ca. $P/P^0 = 0.98$. [d] Diameter of the mesopores corresponding to the maximum of the distribution curve obtained by applying the Barrett, Joyner, and Halenda formula to the desorption branch of the N_2 sorption isotherm.

Once the nanocasting process optimized, to understand the salient features of the nanowires crystallization upon calcination, various in situ X-ray scattering and absorption techniques, accessible at the French synchrotron radiation facility (LURE, Orsay), were used. X-ray absorption near edge spectroscopy (XANES), anomalous wide-angle X-ray scattering (AWAXS), and SAXS measurements were used to check the temperature at which the precursor Mn(II) salt is transformed into $\beta-MnO_2$. We show that the possibility of recording XANES and AWAXS simultaneously, with the same setup and measurement temperature, is an advantage to follow phase transformations. Moreover, we show that simulations can be used to estimate the dimensions of the coherent domains.

Experimental Section

Materials. Chemical analysis data and structural information about SBA-A (mesopore diameter of 4 nm) and SBA-B (mesopore diameter of 6 nm) supports in their blank form, after Mn-loading and after calcination, are gathered in Table 1. As already detailed elsewhere,[19] SBA-A and SBA-B differ by their overall porous volume and mesopore diameters and also in their amount of disordered intrawall micropores. Commercial (Aldrich) manganese salts (chloride and nitrate) and oxide references (Mn_2O_3 and MnO_2) were used as received.

(a) Preparation by Adsorption. The first series of Mn-loaded samples was prepared by adsorption. After the calcination required to eliminate the triblock copolymer used as a templating agent (P_{123}, BASF),[1] the silicas were suspended in

(13) Tseng, T. K.; Chu, H.; Hsu, H. H. *Environ. Sci. Technol.* **2003**, *37*, 171.
(14) Suib, S. L. *Stud. Surf. Sci. Catal.* **1996**, *102*, 47.
(15) Cheast, R. C.; Selby, S. M.; Hodgman, C. D. *Hanbook of Chemistry and Physics*, 46th ed.; The Chemical Rubber Co.: Cleveland, 1965.
(16) (a) Nohman, A. K. H.; Ismail, H. M.; Hussein, G. A. M. *J. Anal. Appl. Pyrolysis* **1995**, *34*, 265. (b) Zaki, M. I.; Nohman, A. K. H.; Hussein, G. A. M.; Nashed, Y. E. *Colloids Surf. A* **1995**, *99*, 247.
(17) Chabre, Y.; Pannetier, J. *Prog. Solid State Chem.* **1995**, *23*, 1−130.
(18) Pham-Huu, C.; Keller, N.; Estournes, C.; Ehret, G.; Ledoux, M. J. *Chem. Commun.* **2002**, 1882.
(19) Imperor-Clerc, M.; Davidson, P.; Davidson, A. *J. Am. Chem. Soc.* **2000**, *122*, 11925.

an aqueous solution containing either manganese chloride or manganese nitrate (constant 10/1 volume/weight ratio, solution containing 23 mmol of Mn per g of silica). After 2 h of contact, the powders were recovered by filtration and then dried in air at room temperature for 48 h. The filtration was aimed at eliminating most of the nonadsorbed manganese species. Ex situ calcination was performed in air in a muffle oven, at a rate of 5 °C·min^{-1} up to 400 °C. The final temperature was maintained for 3 h before cooling down to room temperature. Similar Mn loading and calcination were reproduced with the nonporous silica reference (Aerosil Degussa 380).

(b) Preparation by the "Two Solvents" Method. The second series of Mn-loaded samples was prepared by suspending calcined SBA-A and SBA-B powders in dry *n*-hexane, used as a first solvent. After stirring (15 min, 125 rpm), a small amount of water (second solvent, volume equal to the porous volume of the silica mould, determined by N_2 sorption, typically 1 cm^3 per g of silica) containing dissolved $Mn(NO_3)_2{\cdot}4H_2O$ salt (concentration of 2.34 mmol by cm^3) was added dropwise. The powders were then recovered by filtration and dried in air, still at room temperature. Ex situ calcined samples, necessary for N_2 sorption and TEM experiments, were prepared in a muffle oven at a heating rate of 1 °C/min. The final temperature, 400 °C, was maintained for 3 h before cooling down to room temperature. Uncalcined samples were used directly for in situ X-ray diffraction measurements upon calcination (5 °C/min, in air).

Methods. (a) Elemental Analyses. Analyses were performed by inductive coupling plasma at the CNRS center of chemical analyses (Solaize, France).

(b) TEM Measurements. A JEOL JEM-100 CX II UHR transmission electron microscope operating at 100 keV was used. Samples were prepared either by dispersing the powders in a slurry of dry ethanol, deposited on a copper grid covered with a carbon thin film, or by including within a resin for the preparation of ultrathin sections of the silica grains. In the latter case, a few milligrams of powder were deposited in the bottom of a Beem capsule. Some embedding resin (Epon 812, Roth) was added and polymerized for 48 h at 60 °C. The polymerized blocks were cut using a diamond knife. Ultrathin sections of about 70-nm thick were deposited on copper grids. On these sections, the main axes of the silica grains are randomly oriented. On the images which are presented here, only silica grains cut either parallel to their main axis (longitudinal) or perpendicular to this axis (transversal) were selected. HRTEM images were recorded with magnifications from 33000 up to 470000. The fringes periodicity was measured directly on magnified images. Energy-dispersive X-ray spectroscopy, EDXS, was made using a PGT-IMIX PC system, with an analysis spot of 130 nm in diameter on several regions (at least 3) of the same Mn-loaded silica grain and on several grains (at least 5).

(c) N_2 Sorption. The N_2 sorption isotherms were measured with an ASAP 2010 apparatus (Micromeritics, Norcross). Prior to the experiment, the samples were dehydrated at 50 °C for a few hours and then at 150 °C for more than 6 h under a vacuum better than 10^{-4} Torr. The single-point total pore volume was estimated ca. $P/P^0 = 0.98$. The specific surface area was obtained by using Brunauer−Emmett−Teller equations in the P/P^0 range (0.05−0.25). An estimate of the average diameter of primary mesopores, labeled D_{BJH}, was derived from the maximum of the pore size distribution curve obtained by applying the Barrett−Joyner−Halenda formula to the desorption part of the isotherm, for P/P^0 greater than 0.30. This technique of analysis is known to underestimate mesopore diameters but relative variations among samples should be correct.[20]

(d) X-ray Scattering Measurements. WAXS diffractograms were obtained on a powder Siemens D500 diffractometer using a Cu Kα anticathode. All other X-ray diffraction measurements were made at the LURE synchrotron facility (Orsay, France), on the DCI storage ring running at 1.85 GeV, with an average current of 300 mA and a lifetime of 200 h. XANES and AWAXS measurements were both collected at the H10 experimental station using a heating cell opened to air. More details about the different equipment available on this beam-line can be found in ref 21. XANES spectra were collected at the Mn K edge (6.54 keV) in fluorescence mode. Raw spectra are plotted without any treatment. AWAXS measurements were performed at 6.542 and 6.400 keV. The diffractograms were recorded in a $\theta/2\theta$ step scan mode in the range $q = 1.5-6.0$ Å^{-1} using a NaI scintillation detector. SAXS spectra were collected at the D43 experimental station, using a bent Ge monochromator (111 reflection) to select the wavelength ($\lambda = 0.145$ nm) and focus the beam. The beam size was defined by a collimator of 0.5 mm in diameter. Vacuum flight tubes were inserted between the sample and the detector to get rid of the parasitic air scattering. Powder samples were held in Lindemann glass capillaries of 0.7−1 mm in diameter, either sealed or opened to air. An in situ METTLER heating stage was used to follow the effect of silica dehydration and manganese oxides crystallization upon heating, up to 350 °C. Diffraction patterns in the 0.5−3.0 nm^{-1} q-range were recorded with a CCD camera (Princeton Instrument). Powder diffraction rings were observed and the scattered intensity was azimuthally integrated and plotted as a function of q.

Numerical simulations of the diffractograms expected at different photon energies and with spherical MnO_2 particles of different sizes were performed to help the interpretation of the AWAXS results. First, the size was varied between 15 and 70 Å in diameter and a model of the oxide, here β-MnO_2 (pyrolusite), was selected in view of the diffraction detected at wide angles. Next, all the interatomic distances between ion pairs were calculated. The corresponding diffraction intensities were then calculated from the Debye formula as a function of q and compared to experimental intensities.[22,23]

Results and Discussion

Optimization of the Nanocasting Process. (a) Mn-Loaded Samples Prepared by Adsorption. After the samples were loaded with manganese chloride, the Mn-loaded SBA samples have a light color, ranging from pink to light brown. Chemical analyses show that there are nearly two chloride ions per Mn(II) cation. Therefore, at least at the detection level of chemical analyses (±0.1 on Mn/Cl atomic ratios), the chemical integrity of the salt is preserved upon adsorption. Nearly 7% of the Mn(II) cations, initially present as $Mn(H_2O)_6^{2+}$ complexes in the pink adsorption solution (as demonstrated by electron spin resonance, data not shown), is not eliminated upon filtration on the reference nonporous silica compared to 14% on SBA-A and 28% on SBA-B. This evolution nicely correlates with specific surface areas and porous volumes variations. At a molecular level, in the pH conditions that we have used (pH near 4 whereas the point of zero charge (pzc) of silica ≈2)[24] surface silanol groups are deprotonated. This generates negative charges that most probably induce electrostatic interactions with guest $Mn(H_2O)_6^{2+}$ cations. To check if hydrogen bonds are involved, a SBA-B sample loaded

(20) Galarneau, A.; Cambon, H.; Di Renzo, F.; Fajula, F. *Langmuir* **2001**, *17*, 8328.

(21) Gailhanou, M.; Dubuisson, J. M.; Ribbens, M.; Roussier, L.; Bétaille, D.; Créoff, C.; Lemmonier, M.; Denoyer, J.; Bouillot, C.; Jucha, A.; Lena, A.; Idir, M.; Bessière, M.; Thiaudière, D.; Hennet, L.; Landron, C.; Coutures, J. P. *Nucl. Instrum. Methods A* **2001**, *467−468*, 749.

(22) Revel, R.; Bazin, D.; Dexpert, H.; Elkaim, E.; Seigneurin, A. *J. Phys. Chem. B* **2000**, *104*, 9828.

(23) Bazin, D.; Revel, R. *J. Synchrotron Radiat.* **1999**, *6*, 483.

(24) Brown, J. E., Jr.; Henrich, V. E.; Casey, W. H.; Clark, D. L.; Eggleston, C.; Felmy, A.; Goodman, D. W.; Grätzel, M.; Maciel, G.; McCarthy, M. I.; Nealson, K. H.; Sverjensky, D. A.; Toney, M. F.; Zachara, J. M. *Chem. Rev.* **1999**, *99*, 77.

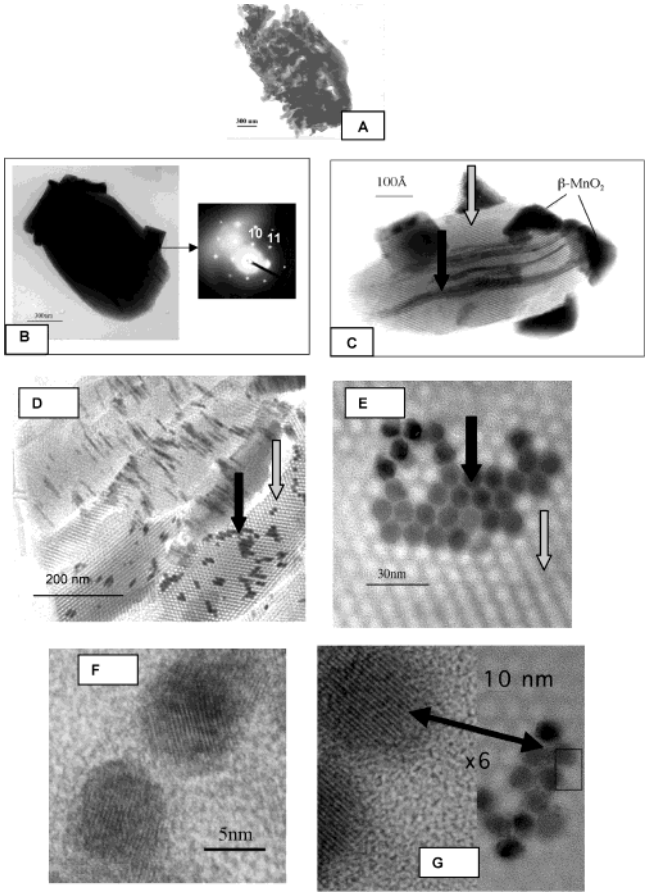

Figure 1. TEM images of Mn-loaded silica samples: (A) nonporous silica reference; (B, D, F) SBA-A and (C, E, G) SBA-B silica grains prepared by adsorption with an aqueous solution of $MnCl_2$, $4H_2O$ (calcination at 5 °C/min until 400 °C, annealing at this temperature for 3 h). This procedure yields a heterogeneous distribution of manganese oxide particles both inside (nanowires) and outside (external particles) the silica grains. (B) A typical SBA-A silica grain (1-μm long, final Mn/Si atomic ratio of 0.20): on this overview a dark and large (larger dimension > 0.25 μm) external crystallite of β-MnO_2 (pyrolusite, JCPDS no. 72-1984, quadratic) was identified by microdiffraction (see insert). (D) Ultrathin section of similar grains: in gray, the preserved two-dimensional hexagonal structure (gray arrow); in black, a heterogeneous distribution of nanowires occluded within the mesopores (black arrow). (F) A magnified region of (D): two sets of reflection planes around 3.35 and 3.54 Å are observed. The fringes of two adjacent nanowires are not correlated (different alignment). (C) Typical SBA-B silica grain (1-μm long, final Mn/Si atomic ratio of 0.40): crystallites of β-MnO_2 on the external surface of the silica grain are also observed. In addition, the silica grain displays longitudinal gray stripes (gray arrow) attributed to empty mesopores and darker stripes due to mesopores filled by manganese oxide nanowires (black arrow). (E) Ultrathin sections of a similar grain. (G) Magnified region of (E) a single set of reflection planes with an interfringe distance of 3.65 Å is observed. The fringes of two adjacent nanowires are correlated (same alignment).

with Mn(II) salt was washed three times with 10 mL of water (per g of silica), ethanol, or acetone. With water, nearly all the manganese species (93%) were eliminated compared to 60% with ethanol and 30% with acetone. A protic and polar solvent is therefore necessary to compete with the H-bonds that maintain the manganese salt on the silica surface.

After calcination, the samples were first characterized by TEM. A heterogeneous deposit surrounds the non-

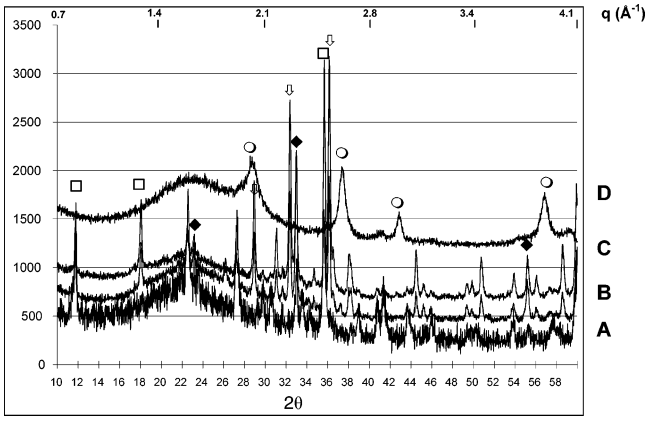

Figure 2. X-ray diffraction at wide angles of Mn-loaded samples obtained by adsorption: (1) of manganese chloride then calcined at 400 °C, (A) Aerosil 380, (B) SBA-A, (C) SBA-B; (2) of manganese nitrate then calcined at 400 °C, (D) on SBA-A. The main diffraction peaks discussed in the text are indicated using different symbols: □ $Mn_8O_{10}Cl_3$ (JCPDS no. 81-2247), ○ β-MnO_2 (JCPDS no. 72-1984), ◆ Mn_2O_3 (JCPDS no. 41-1442), and ↓ Mn_3O_4 (JCPDS no. 80-0382).

porous reference silica grains (Figure 1A). Some chlorine remains (Cl/Mn atomic ratio ≈ 0.5). On X-ray diffractograms collected at wide angles (Figure 2), large peaks due to a manganese oxichloride ($Mn_80_{10}Cl_3$, JCPDS 81-2247, four main diffractions at 7.55, 3.94, 2.52, and 1.54 Å) and α-Mn_2O_3 (bixbyite, JCPDS # 41-1442, main diffractions at 3.83, 2.71, 1.66, and 1.42 Å) are identified (Figure 2A). Very small peaks due to β-MnO_2 (pyrolusite, JCPDS # 72-1984, main diffractions near 3.10, 2.40, and 1.62 Å) are also detected. In contrast, the samples prepared with SBA-A and SBA-B silicas are almost chlorine-free (Cl/Mn atomic ratio <0.1). X-ray diffraction measurements at wide angles mostly indicate the coexistence of α-Mn_2O_3 and Mn_3O_4 (hausmanite, JCPDS # 80-0382, main peaks at 3.08, 2.77, 2.49, and 1.44 Å, Figure 2B and 2C). Interestingly, the integrated intensity ratio of the 2.77 and 2.71 Å diffraction peaks, respectively attributed to Mn_3O_4 and α-Mn_2O_3, is equal to 1.2 on SBA-B and is signicantly smaller on SBA-A (0.8). Small external β-MnO_2 particles attached to the silica grains are identified by TEM microdiffraction (Figure 1B, insert). In addition, longitudinal clear stripes (gray arrow, Figure 1C−1E) corresponding to empty mesopores and black stripes (black arrow) attributed to mesopores filled by MnO_x nanowires can be distinguished in the silica grains. The coexistence of empty and filled mesopores is confirmed by images collected using transversal ultrathin sections (perpendicular to the main axis of the grains, Figure 1D and 1E). As can be seen at higher magnification (Figure 1F and 1G), fringes associated with reticular planes are detected on some of the nanowires. On selected images, two different sets of reticular planes at 3.35 and 3.54 Å associated with α-Mn_2O_3 and a single set of reticular planes at 3.65 Å associated with Mn_3O_4 can be measured.

Another series of samples was prepared in similar conditions using manganese nitrate. By chemical analyses, nearly 2 N atoms were found for each Mn^{II} cation. Therefore, here again, the chemical integrity of the salt is preserved, at least at the detection level of chemical analysis (±0.1 on N/Mn atomic ratios). After ex situ calcination at 400 °C, the diffraction peaks of β-MnO_2

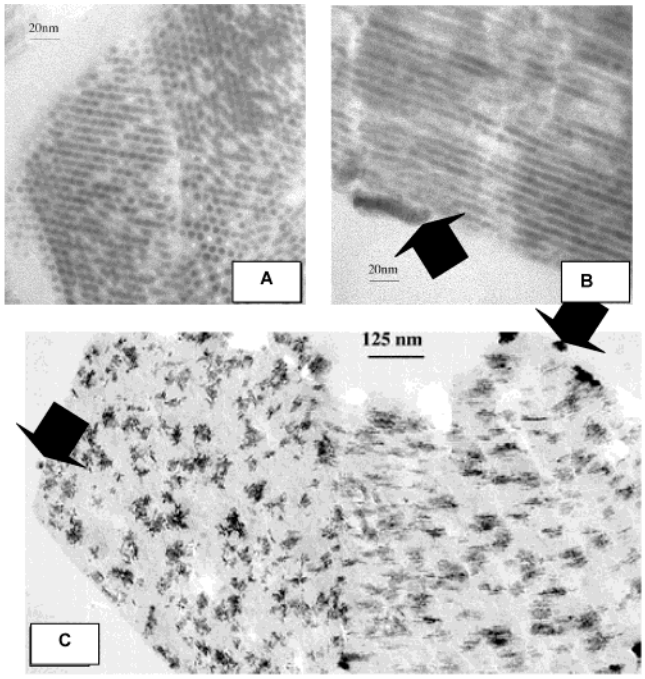

Figure 3. TEM images of ultrathin sections of calcined Mn-loaded SBA-A and SBA-B, silica grains prepared by the "two solvents" technique (atomic Mn/Si ratio of 0.5), in gray silica walls and in black manganese oxide nanowires, (A) longitudinal and (B) transversal sections of a SBA-A silica grain contacted with a volume of aqueous solution set equal to the mesoporous volume, and (C) transversal (left) and longitudinal (right) sections of SBA-B silica grains contacted with the same aqueous solution (same concentration, same volume). The amount of Mn introduced is not large enough for β-MnO_2 nanowires to crystallize everywhere in the porosity, resulting in a speckled image. The black arrows show residual manganese oxide particles grown outside the silica grains.

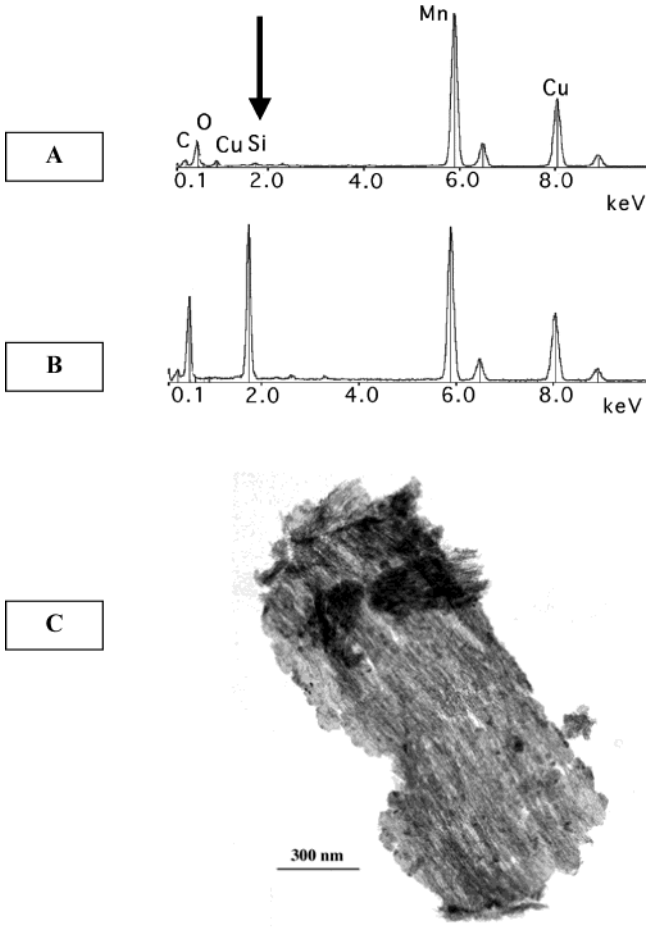

Figure 4. A Mn-loaded SBA-A grain after silica elimination using NaOH treatment: (A) an EDX spectrum showing that the Si atoms are fully eliminated, (B) comparison with an EDX spectrum obtained before silica dissolution, and (C) a TEM image showing the super-lattice formed by connected MnO_2 nanowires. Note the dimensions of a single wire (diameter ca. 5 nm; length ca. 1 μm) and those of the bundle, analogous to that of a SBA-A silica grain (transversal section 300 nm and longitudinal section 1 μm).

are the only ones observed (Figure 2D). These samples are also heterogeneous because they contain the following: (i) both empty and filled mesopores and (ii) a distribution of manganese oxide particles inside and outside the porosity.

(b) Mn-Loaded Samples Prepared by the "Two Solvents" Technique. The TEM images presented in Figure 3 were obtained on ultrathin longitudinal and transversal sections of silica grains loaded with manganese using the "two solvents" technique and then calcined ex situ at 400 °C. On SBA-A grains (Figure 3A and 3B), black MnO_x particles are detected in the mesopores. In N_2 sorption experiments, specific surface area and porous volume are reduced. An important decrease of the porous volume (97%) suggests that the nitrogen molecules can only probe the external surface of the silica grains. This last observation is difficult to analyze in itself because some MnO_x particles, generated by calcination, might block the entrance of the silica mesopores. However, by EDXS, a constant atomic Mn/Si ratio (0.50 ± 0.03) was found on different parts of a given silica grain and, also, on at least 5 different Mn-loaded grains. We can therefore safely consider that the porosity of the SBA-A mould is homogeneously filled with manganese oxide particles in our experimental conditions. A definitive argument for complete filling of the pores is obtained after silica dissolution with NaOH (0.2 M). When silica is fully eliminated (EDX spectra in Figure 4A and 4B), MnO_2 nanowires of 3−4 nm in diameter (for a SBA-15 hard template with mesopores of 4 nm in diameter) and about 1-μm long are revealed by electron microscopy (Figure 4C). These nanowires form a self-supported bundle. Disordered connections between adjacent nanowires should exist and probably derive from the patterning of manganese oxide in the disordered intrawall micropores of the SBA-15 mould, as already demonstrated during the nanocasting of several oxides.[11]

The TEM images obtained on ultrathin sections of SBA-B silica grains have a speckled appearance (Figure 3C). N_2 sorption experiments indicate that 60% of the porous volume is restored after ex situ calcination. EDXS measurements show that atomic Mn/Si ratios vary within the range 0.1−0.9 with an averaged value of 0.5 on 10 silica grains. This suggests that, for an atomic Mn/Si ratio of 0.5, the amount of manganese salt introduced in the porosity of the SBA-B silica is too small to fill it entirely with manganese oxide particles. Since the present study aims at comparing Mn-loaded SBA-A and SBA-B samples of the same Mn/Si atomic ratio, results concerning Mn-loaded SBA-B samples with an occupation volume larger than 60% will not be presented here.

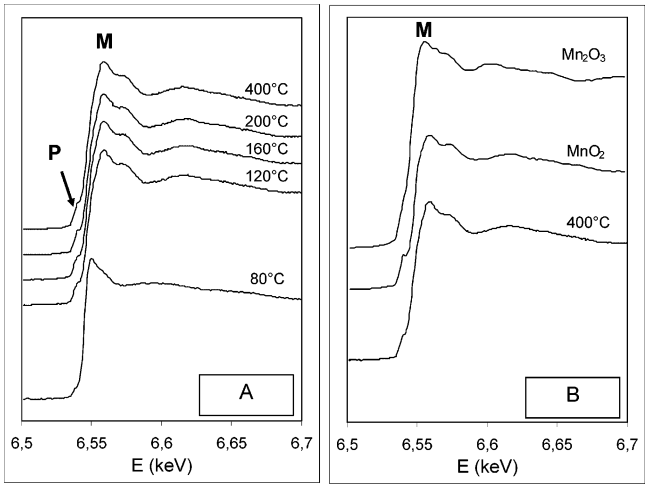

Figure 5. X-ray absorption spectra near the Mn K-edge (XANES): (A) Mn-loaded SBA-B silica upon in situ calcination (from 80 to 400 °C); (B) spectrum obtained at 400 °C compared with those of commercial MnO_2 and Mn_2O_3 reference samples. The spectra were recorded in fluorescence mode, at the same sample and detector angles for all samples. The raw spectra have been shifted along the vertical axis for comparison purposes.

Wide-angle X-ray diffractograms were recorded after ex situ calcination. Several peaks attributed to β-MnO_2 were observed on both the Mn-loaded SBA-A and SBA-B silicas. All these peaks are significantly broader than those of bulk MnO_2 crystallites (full-width at half-maximum of the (101) line of 1.8° on SBA-A and 0.8° on SBA-B, with an instrumental resolution of 0.2°).

Crystallization of Manganese Oxide Nanowires Monitored by X-ray Diffraction Techniques upon in Situ Calcination. In this part, we show that in situ diffraction recorded upon calcination can be used to follow the crystallization of manganese oxide at increasing length scales. XANES gives specific information at the atomic level about the average oxidation state of the manganese species. The crystallization of manganese oxides, the structure, and average size of the crystals can be directly determined by AWAXS. Then, the preservation of the two-dimensional hexagonal structure and the distribution of manganese oxide particles inside the silica matrix can be investigated by SAXS.

(a) XANES. On the spectra presented in Figure 5, two distinct features, typical of manganese ions surrounded by six ligands, are indicated: (i) a P pre-edge peak, arising from dipole forbidden, quadrupole allowed Mn 1s → 3d transitions. This pre-edge is absent for Mn-(II) species. Its intensity is known to decrease if Mn-(IV) ions are reduced to Mn(III) because of distortions introduced by the Jahn−Teller effect; (ii) the main peak M (white line) corresponding to the absorption of X-ray photons at the edge energy of Mn.[25] Between 80 and 120 °C, there is a progressive shift of the M absorption edge toward higher energies and an increase in the intensity of the P pre-edge, indicating that Mn(II) species are oxidized to Mn(IV). The curves recorded between 120 and 400 °C are very similar. In particular, the intensity of the P pre-edge peak remains constant. There is therefore no further thermal reduction of Mn-(IV) species. On Figure 5B, the curve obtained after calcination at 400 °C is compared with the ones obtained on two commercial samples, Mn_2O_3 (III) and MnO_2 (IV), measured in the same experimental conditions. By a simple qualitative comparison, the oxidation state (IV) can be confirmed.

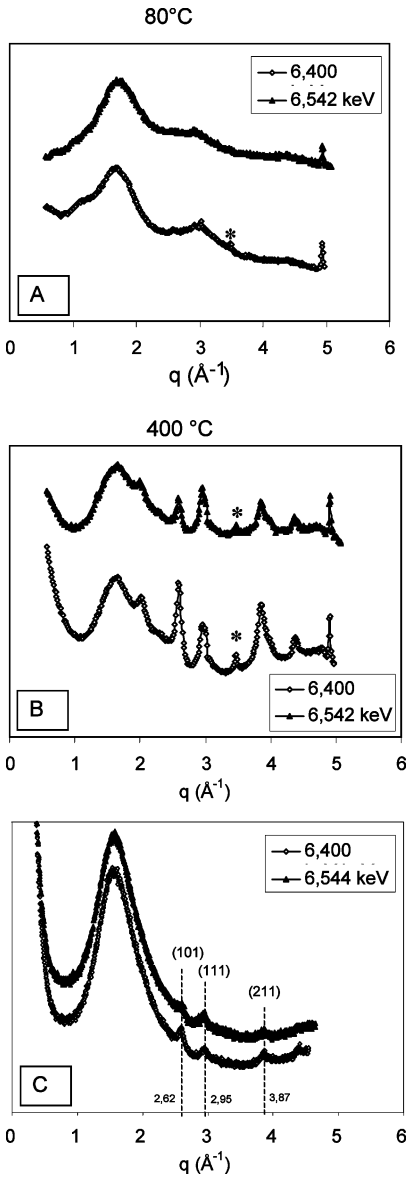

Figure 6. Anomalous wide-angle X-ray scattering for the Mn-loaded SBA-B sample at 80 °C (A), 400 °C (B), and the Mn-loaded SBA-A sample at 400 °C (C). Parasitic narrow diffraction peaks of the stainless steel sample holder are labeled by * symbols.

(b) AWAXS. Figure 6 shows AWAXS measurements performed upon in situ calcination of the Mn-loaded SBA-B sample. At 80 °C (Figure 6A), only a broad diffraction peak attributed to amorphous silica and small peaks due to the stainless steel sample holder (indicated by a * symbol in Figure 6) are recorded. Upon heating, several diffraction peaks due to β-MnO_2 particles appear, in concomitance with the change of oxidation state detected in XANES. These peaks are broader than the experimental resolution, which shows that very small or highly defective crystallites are growing. The diffraction peaks observed at 400 °C can be indexed by assuming a quadratic unit cell with $a =$

(25) Ressler, T.; Brock, S. L.; Wong, J.; Suib, S. L. *J. Phys. Chem. B* **1999**, *103*, 6407.

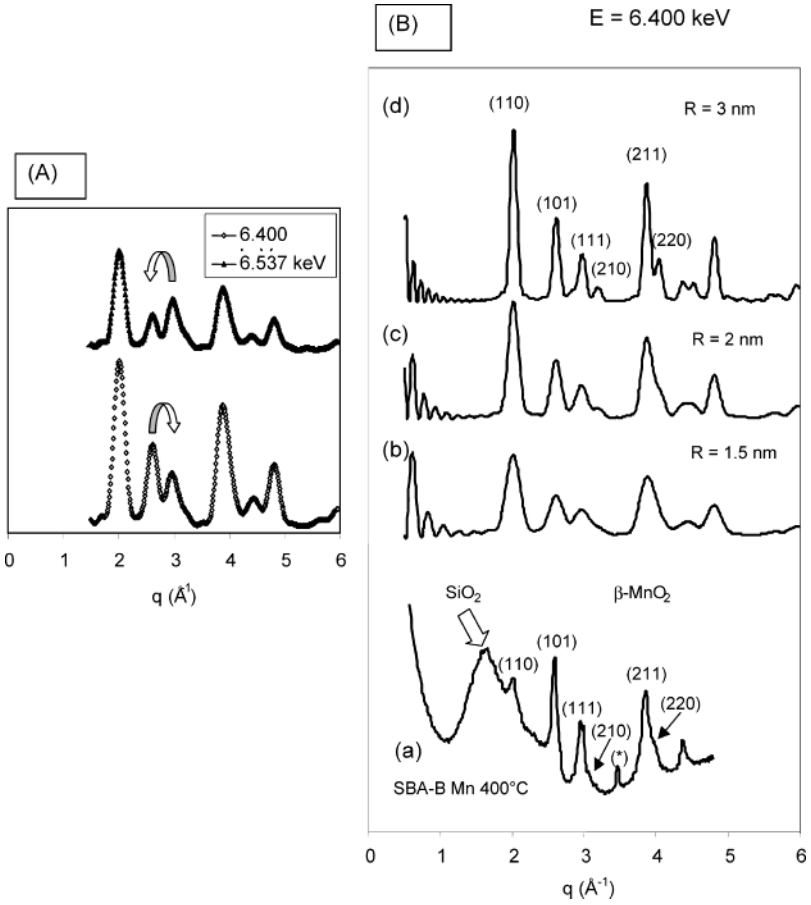

Figure 7. Calculated diffraction for spherical defect-free pyrolusite particles (A) for a radius of 15 Å at two energies, 6.4 and 6.537 keV: a strong anomalous effect is detected on the two peaks indexed (101) and (111); (B) for radii equal to 15 (b), 20 (c), and 30 Å (d), compared to the diffraction observed on a Mn-loaded sample calcined in situ up to 400 °C (a). Depending upon the radius, the (220) peak appears either as a shoulder of the intense (211) diffraction or as a distinct peak.

Table 2. Values of the Two-Dimensional Hexagonal Lattice Parameter before and after Crystallization of MnO_2 Nanowires for Mn-Loaded SBA-A and SBA-B Silica Prepared by the "Two Solvents" Technique and the Deduced Contraction of the Lattice (SAXS Measurement)

a (nm)	blank	Mn-loaded before calcination (nm)	Mn-loaded after calcination (nm)	contraction upon calcination (%)
SBA-B	11.0	11.1	11.0	−0,6
SBA-A	9.6	9.5	9.4	−1,1

4.428 ± 0.029 Å and c = 2.875 ± 0.007 Å unit cell parameters, as expected for pyrolusite, β-MnO_2 (Table 3). However, the a unit cell parameter is a little too large compared to that of perfect pyrolusite. This is indeed expected for defective pyrolusite crystals containing structural defects of ramsdellite type.[14] The presence of pyrolusite, ramsdellite intergrowth is confirmed by other features: the first diffraction peak, indexed (110), is much smaller and broader in experimental diffractograms than in the calculations of the structure factor of pyrolusite that we have performed (Figures 7B and 7C). The observed line width reflects both the small size of the β-MnO_2 particles and the dominant contribution of ramsdellite defects. From the line width, using the method proposed by Chabre and Pannetier,[14] the proportion of ramsdellite defects in β-MnO_2 pyrolusite nanowires was estimated to be ca. 10% in SBA-B. This evaluation was not possible with SBA-A because, with this silica, the (110) diffraction is too broad to be detected. Other peaks, in particular the ones indexed (210) and (220), also deserve attention. On SBA-B, they only appear as shoulders on the more intense (111) and (211) peaks, respectively. On SBA-A, all the diffraction peaks are so broad that these shoulders cannot be detected. This indicates that the MnO_x crystallites formed in a SBA-B mould are significantly larger than those detected in SBA-A (diameter of primary mesopores 7 and 4 nm, respectively).

Table 3. Wide-Angle Diffraction Peaks of MnO_2 for the Mn-Loaded SBA-B Silica Prepared by the Two Solvents Technique, after in Situ Calcination at 400 °C[a]

q_{cal} (Å^{-1})	q_{mes} (Å^{-1})	d_{mes} (Å)	d_{cal} (Å)	*hkl*
2.010	2.011	3.124	3.131	(110)
2.598	2.593	2.423	2.411	(101)
2.843			2.211	(200)
2.961	2.957	2.125	2.118	(111)
3.179	weak	weak	1.981	(210)
3.851	3.858	1.629	1.631	(211)
4.021	weak	weak	1.565	(220)
4.348	4.371	1.437	1.438	(002)
4.495	weak	weak	1.400	(310)

[a] Indexation was done with a quadratic pyrolusite (rutile) unit cell with a = 4.428 ± 0.019 Å and c = 2.875 ± 0.007 Å (chi squared coefficient 2.22 × 10^{-6}). Five peaks are accurately measured and three other are detected but weak.

Simulations were performed using a simple model of defect-free pyrolusite spheres of variable radii (Figure 7). Our simulations reproduce quite well the variation of the relative intensities of the diffraction peaks at the Mn K edge energy, with a strong anomalous effect for

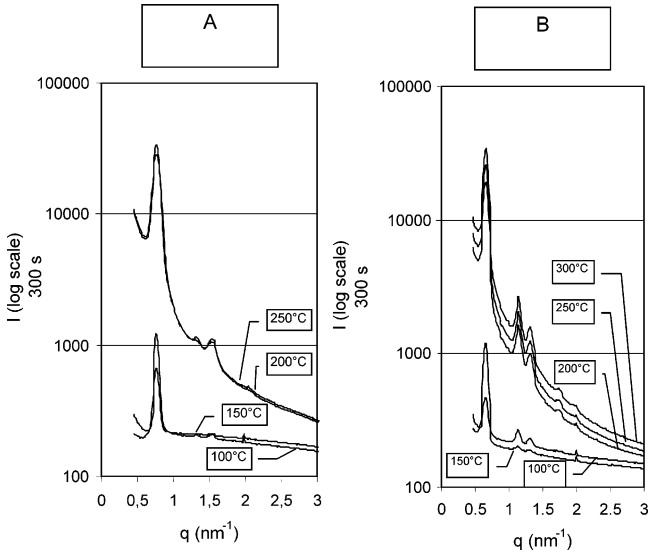

Figure 8. Small-angle scattering results during heating of Mn-loaded (A) SBA-A and (B) SBA-B silicas. Intensity is in logarithmic scale.

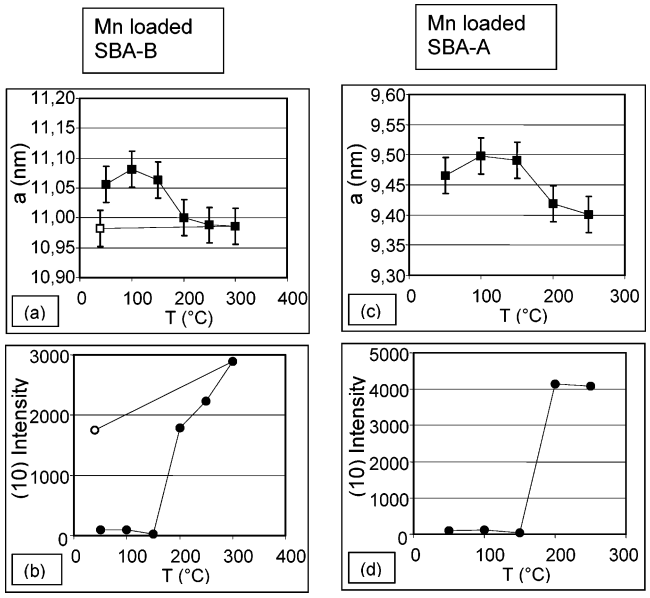

Figure 9. Evolution of the two-dimensional hexagonal lattice parameter versus temperature: (A) for the Mn-loaded SBA-B silica and (C) for the Mn-loaded SBA-A silica; Values of the intensity of the (10) diffraction line in arbitrary units versus temperature: (B) for the Mn-loaded SBA-B silica and (D) for the Mn-loaded SBA-A silica. The point symbolized by a white square has been measured after cooling to room temperature.

the (101) diffraction peak for instance (Figure 7A). We have used these simulations to estimate the dimensions of MnO_2 nanowires. The simulations of Figure 7B indicate that the size of the coherent domains in SBA-B lies between 3 and 6 nm. Indeed, for spheres with radius larger than 3 nm, the (210), (220), (211), and (220) diffraction peaks should be well-separated. Particles are even smaller in SBA-A because, for spheres of radius smaller than 1.5 nm, no shoulder can be attributed to (211) and (220) diffractions. It is important to note that these sizes are very close to the pore size of the silica host estimated by N_2 sorption (radius 3.5 and 2 nm, respectively), which confirms that most of the β-MnO_2 particles are located inside the porosity of the silica hosts.

(c) SAXS. At room temperature, the overall intensity of the diffractograms recorded on uncalcined Mn-loaded SBA-A and SBA-B materials is lower than that observed with blank silicas. The porosity is filled with hydrated Mn(II) species and the resulting electron density contrast between the porosity and silica walls is lower than that of the blank silicas. This overall intensity remains fairly constant below 150 °C. Above this temperature, an abrupt but very small contraction (1%) of the two-dimensional hexagonal lattice is observed (Figures 8 and 9, Table 2). At the same temperature, a clear increase of the overall intensity occurs but the relative intensities of the different peaks are not altered. This intensity increase persists when the sample is cooled to room temperature. The intensity of the (10) peak is directly proportional to the square of the electron density difference between the silica walls, ρ_{wall}, and the material inside the porosity, ρ_{pore}[19]: $I_{(10)} \propto (\rho_{wall} - \rho_{pore})^2$. Estimations of the electron densities involved help to understand the intensity dependence with temperature. The electron density ρ_{wall} is about 0.66 $e^-/Å^3$ (taking a massic density of 2.2 g/cm^3 for bulk amorphous silica) and the electron density of water is 0.33 $e^-/Å^3$. At low temperatures, the electron density difference is quite weak because the hydrated manganese species give an electron density ρ_{pore} close to ρ_{wall} of silica. ρ_{pore} is indeed greater than 0.33 (pure water) and probably less than ρ_{wall}, with $\rho_{wall} - \rho_{pore} \approx 0.1-0.2$ $e^-/Å^3$. Upon heating, ρ_{pore} increases because water is progressively eliminated. At high temperature, if the pores are filled with β-MnO_2 nanowires, a value $\rho_{pore} = 1.48$ $e^-/Å^3$ can be expected (calculated from the unit cell size of pyrolusite given above) and $\rho_{wall} - \rho_{pore} = -0.82$ $e^-/Å^3$. After crystallization, $I_{(10)}$ increases by a factor 20 for the SBA-B sample and by a factor 40 for the SBA-A sample.

The same in situ SAXS measurements upon calcination were first performed on blank SBA-A and SBA-B silicas. From room temperature to 320−350 °C, no increase in the diffraction peaks line width is observed, indicating that the two-dimensional hexagonal ordering is retained. The unit-cell parameter remains constant, in contrast with the Mn-loaded samples for which the crystallization introduces a small contraction of the hexagonal lattice. The positions and the relative intensities of the peaks do not significantly change (in that case, $\rho_{wall} - \rho_{pore} = 0.66$ $e^-/Å^3$).

In addition to the Bragg diffraction peaks, a background decreasing regularly with scattering angle is observed for all samples. This background indicates the existence of large-scale heterogeneities (a few 100 nm), probably related to the shapes and sizes of the silica grains. We have noticed that this background becomes much more important for Mn-loaded samples after crystallization (10 times larger than the one observed upon dehydration of blank silicas). This shows that the presence of the MnO_x particles introduce additional large-scale heterogeneities.

Discussion

The chemical nature, dimension, and crystallinity of the MnO_x nanowires that can be patterned with SBA-15 silicas are affected by (i) the nature of Mn(II) salt (chloride, nitrate) used as a precursor, (ii) the

method used to contact the salt with the silica host (adsorption, "two solvents"), and (iii) the structural parameters (mesopore diameter) of the silica host.

Even if the samples prepared by adsorption of manganese chloride are heterogeneous in nature, clear features can nevertheless be associated with the specific use of mesoporous silicas. A manganese oxychloride is detected with a nonporous silica whereas this intermediate is mainly eliminated with mesoporous SBA-A and SBA-B hosts of larger specific surface areas. Furthermore, mixtures of β-MnO_2, α-Mn_2O_3, and Mn_3O_4 are obtained with SBA-A and SBA-B silicas whereas only β-MnO_2 and α-Mn_2O_3 are detected when a nonporous silica reference is used instead. Under our experimental conditions, the SBA-15 silica hosts appear therefore necessary for the specific formation of Mn_3O_4. It is well-known that Mn_3O_4 can be obtained by thermal decomposition of Mn(II) salts.[26] It is known also that, upon calcination, Mn^{II} salts supported on zeolites transform into mixtures of α-Mn_2O_3 and β-MnO_2[27] and that demanding experimental conditions (thermal treatments at more than 900−950 °C,[28] strong electron irradiation in HR-TEM,[28] or even laser irradiation in the visible range[29]) are necessary to induce the further degradation of β-MnO_2 which leads to mixtures of α-Mn_2O_3 and Mn_3O_4. However, the formation of Mn_3O_4 upon a simple heating treatment at 400 °C in air has seldom been reported. Furthermore, the solid-state reactivity of the MnO_x nanowires formed in the porosity of SBA-15 seems to change when the mesopore dimensions are decreased. Indeed, the relative intensities of the diffraction peaks due to Mn_3O_4 compared to α-Mn_2O_3 are larger (1.2) with SBA-B than with SBA-A (0.8). The origin of this difference is difficult to identify because our Mn-loaded SBA-A and SBA-B samples do not contain the same amount of Mn^{II} salt (atomic Mn/Si ratio of 0.2 and 0.4, respectively).

The samples obtained by manganese nitrate adsorption are less heterogeneous and mainly contain β-MnO_2 as demonstrated by wide-angle X-ray diffraction. The selective formation of this oxide is probably associated with the presence of the NO_3^- anions that can fully oxidize Mn(II) species into Mn(IV) ones in the early steps of calcination.

The samples obtained by using a "two solvents" technique mainly contain β-MnO_2 nanoparticles patterned inside the mesopores. N_2 sorption and TEM-EDXS investigations of ex situ calcined samples show that the porosity of SBA-A is homogeneously filled by MnO_x particles. This conclusion is also supported by the average information provided by X-ray diffraction upon in situ calcination. XANES experiments show that Mn(II) precursors are oxidized to Mn(IV) between 80 and 120 °C, that is, at a much lower temperature than expected for bulk nitrate (200 °C). This observation suggests a confinement effect and confirms the location of the precursor salt in the porosity. WAXS and AWAXS data indicate that pyrolusite nanowires are formed. Numerical simulations performed on AWAXS spectra, using spherical pyrolusite particles, give an estimate of the size of these MnO_2 particles and this parameter is found to be in close agreement with the mesopores diameter of the silica host (5 nm for a silica with mesopores of 6 nm in diameter by N_2 sorption). Ramsdellite structural defects (about 10% volume fraction on SBA-B) are evidenced by the line width of the (110) diffraction peak of pyrolusite and the slightly too large *a* unit cell parameter that can be calculated. All these in situ investigations confirm that MnO_2 nanoparticles are confined in the porosity and indicate that the dimensions of coherent domains are limited by the silica walls. A last argument in favor of the location of the nanowires within the porosity stems from simple volume calculations: neglecting the ramsdellite defects, considering a unit-cell volume of 56.37 $Å^3$ and two manganese atoms per unit cell, the manganese amounts used in our synthesis correspond to an occupation volume of 0.65 cm^3 which is consistent with the porous volume of our silicas determined by N_2 sorption (SBA-A: 0.6; SBA-B: 1.1 cm^3 per g). SAXS measurements were also important at two levels. On one hand, they show that the two-dimensional hexagonal structure is preserved at all the steps of the synthesis and calcination of our Mn-loaded samples. On the other hand, they help identify a small contraction of unit-cell parameter of the SBA-15 lattice, detected at the crystallization temperature of MnO_2 nanowires (we have checked that no significant change of lattice parameter occurs on a reference blank silica versus temperature). Furthermore, the overall diffractogram intensity abruptly increases due to the enhanced electronic contrast between the silica walls and the manganese oxide particles.

Conclusions

The goal of the present study was to define mild reaction conditions to efficiently use the porosity of an SBA-15 silica as a nanoreactor to grow MnO_x nanowires. In a first step, experiments performed on samples prepared by adsorption have helped us to select the best manganese salt precursor (nitrate rather than chloride). The "two solvents" technique that we have then developed is very efficient (97% decrease of porous volume on SBA-A, homogeneous Mn/Si molar ratios in EDXS) and yields, after ex situ calcination at 400 °C, samples that are homogeneous at several levels: (i) a single oxidation state, MnO_2 (XANES) in the single pyrolusite crystalline form (wide angle and AWAXS), (ii) nanoparticles grown mostly within the mesopores (MET) and coherent domains of dimensions limited by the silica host, and (iii) mesopores filled with the same amount of manganese on average (EDXS). SAXS measurements performed in situ, upon calcination, confirms that the two-dimensional hexagonal lattice is preserved throughout the crystallization of β-MnO_2. Furthermore, TEM images obtained after silica dissolution confirm the high level of filling of the porosity: self-supported bundles of β-MnO_2 nanowires are observed. These nanowires have a diameter comparable to that of the silica mesopores and a length comparable to that of the silica grains.

Acknowledgment. The authors thank G. D. Stucky and M. Breysse for their constant help and support. M. Gailhanou is gratefully acknowledged for his help during X-ray diffraction measurements.

CM035353M

(26) Bricker, O. *Am. Mineral.* **1965**, *50*, 1296.
(27) Zaki, M. I.; Hasan, M. A.; Pasupulety, L. *Thermochim. Acta* **1998**, *311*, 97.
(28) Yamada, N.; Ohmasa, M.; Horiuchi, S. *J. Crystallogr.* **1986**, *B42*, 58.
(29) Buciuman, F.; Patcas, F.; Cracium, R.; Zahn, D. R. T. *Phys. Chem. Chem. Phys.* **1999**, *1*, 185.